Performance Analysis of TDOA and FDOA Location by Differential Calibration with Calibration Sources

Li Zhang, Ding Wang, and Ying Wu
Institute of Zhengzhou Information Science and Technology, Zhengzhou, Henan Province 450002, China
Email: zhanglily218@gmail.com; wang_ding814@aliyun.com; hnwuying22@163.com

Abstract —This paper derives the performance equation of the differential calibration algorithm using the time differences of arrival (TDOA) and the frequency differences of arrival (FDOA) with calibration sources when the positions and velocities of the receivers have random errors. By comparing the performance with the Cramér-Rao lower bound (CRLB), it proves that the ability of the differential calibration algorithm to restrain these errors depends heavily on the parameters of the calibration sources. Then the influences of their amount, positions and measurement accuracy to the location accuracy are discussed. Simulations corroborate the theoretical results in this paper.

Index Terms—Receiver position and velocity errors, passive location, CRLB, error calibration

I. Introduction

Passive source location has been deeply discussed due to its wide use in various applications including radar, sonar and sensor networks. The focuses of these research efforts are mainly on two points. One is to find optimal methods of solving the equations established under different location scenarios [1]-[3]. The other is to analyze the performance of some practical location systems and restrain the drawbacks which degrade the accuracy [4]-[7]. The study of this paper belongs to the latter.

The performance of several location systems, such as locating the unknown emitter by moving receivers or via non-cooperative receivers, depends heavily on the availability of accurate receiver location parameters. Ref. [5] investigated the loss in the time differences of arrival (TDOA) and the frequency differences of arrival (FDOA) based location accuracy when the available receiver positions and velocities have random errors. By explicitly taking the statistics of the receiver location errors into account, it developed an improved closed-form algorithm which can achieve the Cramér-Rao lower bound (CRLB) accuracy for far-field emitters under Gaussian distributed noise. Ref. [6] and [7] investigated the differential calibration algorithm for satellite uplink signal location in the presence of satellite location errors.

However, [8] showed through geometrical analysis that the differential calibration algorithm using TDOA measurements with a single calibration source could not be always effective to restrain the receiver position error. The fatal factor lies in the position of the calibration source. Furthermore, [6] and [7] showed through simulations that the amount and the positions of the calibration sources played a very important role on the performance of the algorithms they proposed.

This paper extends the work in [6]-[8] and derives the explicit performance equation to analyze the effect of the differential calibration algorithms for receiver location error restraint. The opinion of performance gain over the original CRLB accuracy without any calibration source is first proposed to measure the effect of receiver location error restraint in this paper. The contents of this paper are organized as follows. Section II formulates the problem. Section III presents the performance analysis of the differential calibration algorithm. Section IV provides the simulations and section V concludes the paper.

II. Location Model

A. TDOA and FDOA Measurement Equations

Consider the passive location scenario shown in Fig. 1. N moving receivers and M fixed calibration sources are used to estimate the position and velocity of an unknown emitter. Let $\mathbf{u}=[x \quad y \quad z]^T$ and $\mathbf{v}=[v_x \quad v_y \quad v_z]^T$ be the true position and velocity of it, where $[\bullet]^T$ denotes matrix transpose. $\mathbf{s}_i=[x_i \quad y_i \quad z_i]^T$ is the true position of the $ith, i=1,2,\cdots,N$ receiver and $\mathbf{v}_i=[v_{xi} \quad v_{yi} \quad v_{zi}]^T$ is the velocity. $\mathbf{c}_j=[c_{xj} \quad c_{yj} \quad c_{zj}]^T$ is the true position of the $jth, j=1,2,\cdots,M$ calibration source.

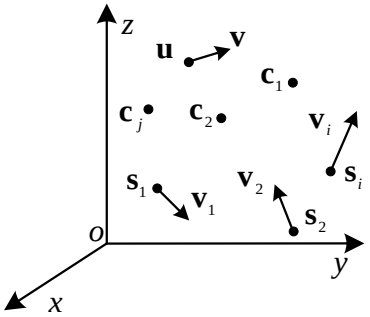

Fig. 1. Location scenario.

Manuscript received March 25, 2014; revised June 27, 2014.
This work was supported by the National Natural Science Foundation of China under Grant No. 61201381.
Corresponding author email: zhanglily218@gmail.com.
doi:10.12720/jcm.9.6.483-489

In reality, the true receiver positions and velocities are not known and only noisy versions of them are available. We represent them as $\tilde{\mathbf{s}}_i = \mathbf{s}_i + \mathbf{d}_i$ and $\tilde{\mathbf{v}}_i = \mathbf{v}_i + \mathbf{w}_i$. The noises $\mathbf{d}_i$ and $\mathbf{w}_i$ are assumed to be mutually independent zero mean Gaussian random vectors.

The true range from the unknown to the *ith* receiver is $r_i = \left\|\mathbf{u} - \tilde{\mathbf{s}}_i + \mathbf{d}_i\right\|$ and its derivative with respect to t is $\dot{r}_i = (\mathbf{v} - \tilde{\mathbf{v}}_i + \mathbf{w}_i)^T \mathbf{b}_i$, where $\mathbf{b}_i = (\mathbf{u} - \tilde{\mathbf{s}}_i + \mathbf{d}_i)/r_i$, $\|\bullet\|$ is Euclidean norm. Those from the *jth* calibration source are $r_{ji} = \left\|\mathbf{c}_j - \tilde{\mathbf{s}}_i + \mathbf{d}_i\right\|$ and $\dot{r}_{ji} = -(\tilde{\mathbf{v}}_i - \mathbf{w}_i)^T \mathbf{b}_{cji}$, where $\mathbf{b}_{cji} = (\mathbf{c}_j - \tilde{\mathbf{s}}_i + \mathbf{d}_i)/r_{ji}$. Then, the TDOA and FDOA measurement equations are

$$r_{uk} = r_{k+1} - r_1 = c(\tilde{\tau}_k - n_k) \tag{1}$$

$$\dot{r}_{uk} = \dot{r}_{k+1} - \dot{r}_1 = \lambda(\Delta\tilde{f}_k - \eta_k) \tag{2}$$

$$r_{cjk} = r_{j(k+1)} - r_{j1} = c(\tilde{\tau}_{cjk} - n_{cjk}) \tag{3}$$

$$\dot{r}_{cjk} = \dot{r}_{j(k+1)} - \dot{r}_{j1} = \lambda(\Delta\tilde{f}_{cjk} - \eta_{cjk}) \tag{4}$$

where $k = 1, 2, \cdots, N-1$, c and λ are the propagation speed and the wavelength of the signal respectively. $\tilde{\tau}_k = \tau_k + n_k$, $\Delta\tilde{f}_k = \Delta f_k + \eta_k$, $\tilde{\tau}_{cjk} = \tau_{cjk} + n_{cjk}$ and $\Delta\tilde{f}_{cjk} = \Delta f_{cjk} + \eta_{cjk}$ are noisy TDOA and FDOA measurements. The noises n_k, η_k, n_{cjk} and η_{cjk} are assumed to be zero mean Gaussian random variables.

B. Mathematical Model of Differencial Calibration

For all the possible values of k and j, we represent the range difference measurements from the unknown emitter by the vector $\tilde{\mathbf{r}} = c[\tilde{\tau}_1 \quad \tilde{\tau}_2 \quad \cdots \quad \tilde{\tau}_{N-1}]^T = \mathbf{r} + c\mathbf{n}$ and represent those from the calibration sources by $\tilde{\mathbf{r}}_c = c[\tilde{\tau}_{c11} \quad \tilde{\tau}_{c12} \quad \cdots \quad \tilde{\tau}_{cM(N-1)}]^T = \mathbf{r}_c + c\mathbf{n}_c$, where the true range difference vectors are $\mathbf{r} = [r_{u1} \quad r_{u2} \quad \cdots \quad r_{u(N-1)}]^T$ and $\mathbf{r}_c = [r_{c11} \quad \cdots \quad r_{cjk} \quad \cdots \quad r_{cM(N-1)}]^T$. The measurement noise vectors are $\mathbf{n} = [n_1 \quad n_2 \quad \cdots \quad n_{N-1}]^T$ and $\mathbf{n}_c = [n_{c11} \quad n_{c12} \quad \cdots \quad n_{cM(N-1)}]^T$ with the covariance matrices $\mathbf{Q}_t$ and $\mathbf{Q}_{tc}$.

Correspondingly, we represent the range difference differential measurements by $\tilde{\dot{\mathbf{r}}}$ and $\tilde{\dot{\mathbf{r}}}_c$ which can be written as $\tilde{\dot{\mathbf{r}}} = \lambda[\Delta\tilde{f}_1 \quad \Delta\tilde{f}_2 \quad \cdots \quad \Delta\tilde{f}_{N-1}]^T = \dot{\mathbf{r}} + \lambda\boldsymbol{\eta}$ and $\tilde{\dot{\mathbf{r}}}_c = \lambda[\Delta\tilde{f}_{c11} \quad \Delta\tilde{f}_{c12} \quad \cdots \quad \Delta\tilde{f}_{cM(N-1)}]^T = \dot{\mathbf{r}}_c + \lambda\boldsymbol{\eta}_c$. $\dot{\mathbf{r}}$ and $\dot{\mathbf{r}}_c$ represent the true values. $\boldsymbol{\eta} = [\eta_1 \quad \eta_2 \quad \cdots \quad \eta_{N-1}]^T$ and $\boldsymbol{\eta}_c = [\eta_{c11} \quad \eta_{c12} \quad \cdots \quad \eta_{cM(N-1)}]^T$ represent the noises with the covariance matrices $\mathbf{Q}_f$ and $\mathbf{Q}_{fc}$.

Rewrite the equations from (1) to (4) as

$$\begin{cases} \boldsymbol{\alpha} = \tilde{\boldsymbol{\alpha}} - \mathbf{e} \\ \boldsymbol{\alpha}_c = \tilde{\boldsymbol{\alpha}}_c - \mathbf{e}_c \end{cases} \tag{5}$$

where $\boldsymbol{\alpha} = [\mathbf{r}^T \quad \dot{\mathbf{r}}^T]^T$, $\boldsymbol{\alpha}_c = [\mathbf{r}_c^T \quad \dot{\mathbf{r}}_c^T]^T$, $\mathbf{e} = [c\mathbf{n}^T \quad \lambda\boldsymbol{\eta}^T]^T$, and $\mathbf{e}_c = [c\mathbf{n}_c^T \quad \lambda\boldsymbol{\eta}_c^T]^T$. Subtracting the $N-1$ equations corresponding to the *jth* calibration source in the lower part of (5) from the upper part of (5) and repeating the operation M times yield

$$\boldsymbol{\alpha}_{dc} = \tilde{\boldsymbol{\alpha}}_{dc} - \mathbf{e}_{dc} \tag{6}$$

where

$$\begin{aligned} \boldsymbol{\alpha}_{dc} &= \mathbf{R}_c\boldsymbol{\alpha} - \boldsymbol{\alpha}_c \\ \mathbf{R}_c &= \begin{bmatrix} \mathbf{1}_{M\times1} \otimes \mathbf{I}_{N-1} & \mathbf{0}_{M\times1} \otimes \mathbf{I}_{N-1} \\ \mathbf{0}_{M\times1} \otimes \mathbf{I}_{N-1} & \mathbf{1}_{M\times1} \otimes \mathbf{I}_{N-1} \end{bmatrix} \\ \tilde{\boldsymbol{\alpha}}_{dc} &= \mathbf{R}_c\tilde{\boldsymbol{\alpha}} - \tilde{\boldsymbol{\alpha}}_c \\ \mathbf{e}_{dc} &= \mathbf{R}_c\mathbf{e} - \mathbf{e}_c, \end{aligned}$$

and $\otimes$ is Kronecher product. $\mathbf{1}_{M\times1}$ and $\mathbf{0}_{M\times1}$ are column vectors with all one and all zero elements respectively.

III. Differential Calibration Algorithm

Some additive system errors in practical location systems, such as the time errors and the frequency errors existing in different receivers, can be removed by differential calibration obviously. In this section, we will investigate the ability of differential calibration to restrain the receiver location errors.

A. Algorithm

As described in section II, we represent the noisy locations of the receivers by the vector $\tilde{\boldsymbol{\beta}} = \boldsymbol{\beta} + \mathbf{n}_\beta$, where $\boldsymbol{\beta} = [\mathbf{s}_1^T \quad \cdots \quad \mathbf{s}_N^T \quad \mathbf{v}_1^T \quad \cdots \quad \mathbf{v}_N^T]^T$ has the true values, $\mathbf{n}_\beta = [\mathbf{d}_1^T \quad \cdots \quad \mathbf{d}_N^T \quad \mathbf{w}_1^T \quad \cdots \quad \mathbf{w}_N^T]^T$ is the noise vector with the covariance matrix $\mathbf{Q}_\beta$. $\mathbf{n}$, $\boldsymbol{\eta}$, $\mathbf{n}_c$, $\boldsymbol{\eta}_c$ and $\mathbf{n}_\beta$ are mutually independent.

Suppose $\boldsymbol{\theta} = [\mathbf{u}^T \quad \mathbf{v}^T]^T$ and $\boldsymbol{\Theta} = [\boldsymbol{\theta}^T \quad \boldsymbol{\beta}^T]^T$. Expand $\boldsymbol{\alpha}_{dc}$ and $\boldsymbol{\beta}$ around $\boldsymbol{\Theta}_0$ in Taylor's series. Keeping only the terms below second order yields

$$\hat{\boldsymbol{\alpha}}_d + \hat{\mathbf{J}}\boldsymbol{\delta} = \tilde{\boldsymbol{\alpha}}_d - \mathbf{e}_d \tag{7}$$

where $\boldsymbol{\delta} = \boldsymbol{\Theta} - \boldsymbol{\Theta}_0$, $\hat{\boldsymbol{\alpha}}_d = [\boldsymbol{\alpha}_{dc}^T \quad \boldsymbol{\beta}^T]^T\big|_{\theta_0,\beta_0}$, $\tilde{\boldsymbol{\alpha}}_d = [\tilde{\boldsymbol{\alpha}}_{dc}^T \quad \tilde{\boldsymbol{\beta}}^T]^T$, $\mathbf{e}_d = [\mathbf{e}_{dc}^T \quad \mathbf{n}_\beta^T]^T$. $\hat{\mathbf{J}}$ is the sample of the Jacobian matrix $\mathbf{J} = \begin{bmatrix} \mathbf{R}_c\mathbf{A} & \mathbf{R}_c\mathbf{D} - \mathbf{D}_c \\ \mathbf{0}_{6N\times6} & \mathbf{I}_{6N} \end{bmatrix}$ at $\boldsymbol{\Theta}_0$ and the partial derivatives are defined as $\mathbf{A} = \partial\boldsymbol{\alpha}/\partial\boldsymbol{\theta}$, $\mathbf{D} = \partial\boldsymbol{\alpha}/\partial\boldsymbol{\beta}$ and $\mathbf{D}_c = \partial\boldsymbol{\alpha}_c/\partial\boldsymbol{\beta}$ whose values are listed in Appendix A.

Applying the best linear unbiased estimator (BLUE) [9] of $\boldsymbol{\Theta}$ from (7) yields the best location accuracy for differential calibration which can be represented as

$$\mathrm{cov}(\boldsymbol{\Theta}) = (\mathbf{J}^T\mathbf{Q}_d^{-1}\mathbf{J})^{-1} \tag{8}$$

where

$$\mathbf{Q}_d = E\{\mathbf{e}_d\mathbf{e}_d^T\} = \begin{bmatrix} \mathbf{Q}_{d\alpha} & \mathbf{0}_{2M(N-1)\times6N} \\ \mathbf{0}_{6N\times2M(N-1)} & \mathbf{Q}_\beta \end{bmatrix}$$

$$\mathbf{Q}_{d\alpha} = E\{\mathbf{e}_{dc}\mathbf{e}_{dc}^T\} = \mathbf{R}_c\mathbf{Q}_\alpha\mathbf{R}_c^T + \mathbf{Q}_c$$

$$\mathbf{Q}_\alpha = \begin{bmatrix} c^2\mathbf{Q}_t & \mathbf{0}_{(N-1)\times(N-1)} \\ \mathbf{0}_{(N-1)\times(N-1)} & \lambda^2\mathbf{Q}_f \end{bmatrix}$$

$$\mathbf{Q}_c = \begin{bmatrix} c^2\mathbf{Q}_{tc} & \mathbf{0}_{M(N-1)\times M(N-1)} \\ \mathbf{0}_{M(N-1)\times M(N-1)} & \lambda^2\mathbf{Q}_{fc} \end{bmatrix}.$$

B. Performance Equation

Using the method similar to [8], we can get the Fisher matrix $\mathbf{F}$ under the location scenario as shown in Fig. 1.

$$\mathbf{F} = \mathbf{H}^T\mathbf{Q}^{-1}\mathbf{H}. \tag{9}$$

where

$$\mathbf{Q} = \begin{bmatrix} \mathbf{Q}_\alpha & \mathbf{0}_{2(N-1)\times 6N} & \mathbf{0}_{2(N-1)\times 2M(N-1)} \\ \mathbf{0}_{6N\times 2(N-1)} & \mathbf{Q}_\beta & \mathbf{0}_{6N\times 2M(N-1)} \\ \mathbf{0}_{2M(N-1)\times 2(N-1)} & \mathbf{0}_{2M(N-1)\times 6N} & \mathbf{Q}_c \end{bmatrix}$$

$$\mathbf{H}^T = \begin{bmatrix} \mathbf{A}^T & \mathbf{0}_{6\times 6N} & \mathbf{0}_{6\times 2M(N-1)} \\ \mathbf{D}^T & \mathbf{I}_{6N} & \mathbf{D}_c^T \end{bmatrix}.$$

Suppose

$$\mathbf{V} = \begin{bmatrix} \mathbf{R}_c & \mathbf{0}_{2M(N-1)\times 6N} & -\mathbf{I}_{2M(N-1)} \\ \mathbf{0}_{6N\times 2(N-1)} & \mathbf{I}_{6N} & \mathbf{0}_{6N\times 2M(N-1)} \end{bmatrix}.$$

Substituting $\mathbf{J} = \mathbf{VH}$ and $\mathbf{Q}_d = \mathbf{VQV}^T$ in (8) and taking the inverse of (8) yield

$$\mathbf{F}_d = \mathrm{cov}(\boldsymbol{\Theta})^{-1} = \mathbf{H}^T\mathbf{V}^T(\mathbf{VQV}^T)^{-1}\mathbf{VH}. \tag{10}$$

Subtracting $\mathbf{F}_d$ from $\mathbf{F}$ yields $\mathbf{F}_d = \mathbf{F} - \mathbf{H}^T\mathbf{BH}$, where $\mathbf{B} = \mathbf{Q}^{-1} - \mathbf{V}^T(\mathbf{VQV}^T)^{-1}\mathbf{V}$. Applying the values of $\mathbf{V}$ and $\mathbf{Q}$ in matrix $\mathbf{B}$ yields

$$\mathbf{B} = \begin{bmatrix} \mathbf{Q}_\alpha^{-1} - \mathbf{R}_c^T\mathbf{Q}_{d\alpha}^{-1}\mathbf{R}_c & \mathbf{0}_{2(N-1)\times 6N} & \mathbf{R}_c^T\mathbf{Q}_{d\alpha}^{-1} \\ \mathbf{0}_{6N\times 2(N-1)} & \mathbf{0}_{6N\times 6N} & \mathbf{0}_{6N\times 2M(N-1)} \\ \mathbf{Q}_{d\alpha}^{-1}\mathbf{R}_c & \mathbf{0}_{2M(N-1)\times 6N} & \mathbf{Q}_c^{-1} - \mathbf{Q}_{d\alpha}^{-1} \end{bmatrix}. \tag{11}$$

Substituting $\mathbf{Q}_{d\alpha}^{-1} = \mathbf{Q}_c^{-1} - \mathbf{Q}_c^{-1}\mathbf{R}_c(\mathbf{Q}_\alpha^{-1} + \mathbf{R}_c^T\mathbf{Q}_c^{-1}\mathbf{R}_c)^{-1}\mathbf{R}_c^T\mathbf{Q}_c^{-1}$ [10] in (11) yields

$$\mathbf{Q}_\alpha^{-1} - \mathbf{R}_c^T\mathbf{Q}_{d\alpha}^{-1}\mathbf{R}_c = \mathbf{Q}_\alpha^{-1}(\mathbf{Q}_\alpha^{-1} + \mathbf{L}_{cc})^{-1}\mathbf{Q}_\alpha^{-1} \tag{12}$$

$$\mathbf{Q}_c^{-1} - \mathbf{Q}_{d\alpha}^{-1} = \mathbf{Q}_c^{-1}\mathbf{R}_c(\mathbf{Q}_\alpha^{-1} + \mathbf{L}_{cc})^{-1}\mathbf{R}_c^T\mathbf{Q}_c^{-1} \tag{13}$$

$$\mathbf{R}_c^T\mathbf{Q}_{d\alpha}^{-1} = \mathbf{Q}_\alpha^{-1}(\mathbf{Q}_\alpha^{-1} + \mathbf{L}_{cc})^{-1}\mathbf{R}_c^T\mathbf{Q}_c^{-1} \tag{14}$$

$$\mathbf{Q}_{d\alpha}^{-1}\mathbf{R}_c = (\mathbf{R}_c^T\mathbf{Q}_{d\alpha}^{-1})^T = \mathbf{Q}_c^{-1}\mathbf{R}_c(\mathbf{Q}_\alpha^{-1} + \mathbf{L}_{cc})^{-1}\mathbf{Q}_\alpha^{-1} \tag{15}$$

$$\mathbf{B} = \boldsymbol{\gamma}^T\mathbf{Q}_{Rc}^{-1}\boldsymbol{\gamma} \tag{16}$$

where $\mathbf{L}_{cc} = \mathbf{R}_c^T\mathbf{Q}_c^{-1}\mathbf{R}_c$, $\boldsymbol{\gamma} = [\mathbf{Q}_\alpha^{-1} \quad \mathbf{0}_{2(N-1)\times 6N} \quad \mathbf{R}_c^T\mathbf{Q}_c^{-1}]$ and $\mathbf{Q}_{Rc} = \mathbf{Q}_\alpha^{-1} + \mathbf{L}_{cc}$ is positive definite if $\mathbf{Q}_\alpha$ is positive definite.

Thus, $\mathbf{F}_d$ can be represented as

$$\mathbf{F}_d = \mathbf{F} - \mathbf{U}^T\mathbf{Q}_{Rc}^{-1}\mathbf{U} \tag{17}$$

where $\mathbf{U} = \boldsymbol{\gamma}\mathbf{H}$. Because $\mathbf{Q}_{Rc}$ is positive definite, the second term in (17) is positive semi-definite.

Suppose $\mathbf{L}_1 = [\mathbf{A} \quad \mathbf{D}]$ and $\mathbf{L}_2 = [\mathbf{0}_{2M(N-1)\times 6} \quad \mathbf{D}_c]$. The former represents the relative relationships of the location among the unknown emitter and the receivers. And the latter represents those among the calibration sources and the receivers. Let $\mathbf{F}_s$ be the Fisher matrix without calibration sources and $\mathbf{F}$ can be represented as

$$\mathbf{F} = \mathbf{F}_s + \mathbf{L}_2^T\mathbf{Q}_c^{-1}\mathbf{L}_2 \tag{18}$$

If $\mathbf{Q}_c$ is positive definite, the second term in (18) is positive semi-definite too.

Substituting $\mathbf{U} = \mathbf{Q}_\alpha^{-1}\mathbf{L}_1 + \mathbf{R}_c^T\mathbf{Q}_c^{-1}\mathbf{L}_2$ and $\mathbf{F}$ in (17) yields

$$\begin{aligned}\mathbf{F}_d = \mathbf{F}_s &+ \mathbf{L}_2^T\mathbf{Q}_{d\alpha}^{-1}\mathbf{L}_2 - \mathbf{L}_1^T\mathbf{Q}_\alpha^{-1}\mathbf{Q}_{Rc}^{-1}\mathbf{Q}_\alpha^{-1}\mathbf{L}_1 - \\ &\mathbf{L}_2^T\mathbf{Q}_c^{-1}\mathbf{R}_c\mathbf{Q}_{Rc}^{-1}\mathbf{Q}_\alpha^{-1}\mathbf{L}_1 - \mathbf{L}_1^T\mathbf{Q}_\alpha^{-1}\mathbf{Q}_{Rc}^{-1}\mathbf{R}_c^T\mathbf{Q}_c^{-1}\mathbf{L}_2\end{aligned} \tag{19}$$

C. Performance Analysis

Taking the inverse of (17) and (18) [10] yields

$$\mathbf{F}^{-1} = \mathbf{F}_d^{-1} - \mathbf{F}_d^{-1}\mathbf{U}^T(\mathbf{Q}_{Rc} + \mathbf{U}\mathbf{F}_d^{-1}\mathbf{U}^T)^{-1}\mathbf{U}\mathbf{F}_d^{-1} \tag{20}$$

$$\mathbf{F}^{-1} = \mathbf{F}_s^{-1} - \mathbf{F}_s^{-1}\mathbf{L}_2^T(\mathbf{Q}_c + \mathbf{L}_2\mathbf{F}_s^{-1}\mathbf{L}_2^T)^{-1}\mathbf{L}_2\mathbf{F}_s^{-1} \tag{21}$$

Because the second terms in (20) and (21) are positive semi-definite, the relationships among $\mathbf{F}^{-1} = CRLB(\boldsymbol{\Theta})$, $\mathbf{F}_s^{-1} = CRLB(\boldsymbol{\Theta})_s$ and $\mathbf{F}_d^{-1} = \mathrm{cov}(\boldsymbol{\Theta})$ can be represented as

$$\begin{cases} tr(\mathbf{PF}^{-1}\mathbf{P}^T) \le tr(\mathbf{PF}_d^{-1}\mathbf{P}^T) \\ tr(\mathbf{PF}^{-1}\mathbf{P}^T) \le tr(\mathbf{PF}_s^{-1}\mathbf{P}^T) \end{cases} \tag{22}$$

where $\mathbf{P} = [\mathbf{I}_6 \quad \mathbf{0}_{6\times 6N}]$, $tr(\bullet)$ denotes matrix trace.

As $CRLB(\boldsymbol{\theta}) = tr(\mathbf{PF}^{-1}\mathbf{P}^T)$, $CRLB(\boldsymbol{\theta})_s = tr(\mathbf{PF}_s^{-1}\mathbf{P}^T)$ and $\mathrm{cov}(\boldsymbol{\theta}) = tr(\mathbf{PF}_d^{-1}\mathbf{P}^T)$, (22) shows that the location accuracy with calibration sources is the best one when $\mathbf{Q}_\alpha$ and $\mathbf{Q}_c$ is positive definite. Such conditions are fulfilled without doubt in realistic location systems.

Equation (21) shows the use of calibration sources will not degrade the original location accuracy. If calibration sources are used properly, they will provide performance gain. And their amount, positions and measurement statistics will influence the quantity of the gain.

Though the location accuracy of differential calibration will not be better than $CRLB(\boldsymbol{\theta})$, (19) shows it could be worse than $CRLB(\boldsymbol{\theta})_s$ under some circumstances where the positions and measurement statistics of calibration sources are badly designed. The reason lies in the subtraction operation shown in (6) which mixes the effects from the unknown emitter, the receivers and the calibration sources together.

Substituting $\mathbf{J}$ and $\mathbf{Q}_d$ in (8) yields

$$\mathrm{cov}(\mathbf{\Theta}) = \begin{bmatrix} \mathbf{X}_{dc} & \mathbf{Y}_{dc} \\ \mathbf{Y}_{dc}^T & \mathbf{Z}_{dc} \end{bmatrix}^{-1} \quad (23)$$

$$\mathbf{X}_{dc} = (\mathbf{R}_c\mathbf{A})^T \mathbf{Q}_{d\alpha}^{-1} (\mathbf{R}_c\mathbf{A}) \quad (24)$$

$$\mathbf{Y}_{dc} = (\mathbf{R}_c\mathbf{A})^T \mathbf{Q}_{d\alpha}^{-1} (\mathbf{R}_c\mathbf{D} - \mathbf{D}_c) \quad (25)$$

$$\mathbf{Z}_{dc} = \mathbf{Q}_{\beta}^{-1} + (\mathbf{R}_c\mathbf{D} - \mathbf{D}_c)^T \mathbf{Q}_{d\alpha}^{-1} (\mathbf{R}_c\mathbf{D} - \mathbf{D}_c) \quad (26)$$

The upper left 6×6 block of (23) is

$$\mathrm{cov}(\boldsymbol{\theta}) = (\mathbf{X}_{dc} - \mathbf{Y}_{dc}\mathbf{Z}_{dc}^{-1}\mathbf{Y}_{dc}^T)^{-1} \quad (27)$$

Substituting $\mathbf{Q}_{d\alpha}^{-1}$ in $\mathbf{X}_{dc}$ yields

$$\mathbf{X}_{dc} = \mathbf{A}^T \cdot \mathbf{Q}_{\alpha}^{-1} (\mathbf{Q}_{\alpha}^{-1} + \mathbf{R}_c^T \mathbf{Q}_c^{-1} \mathbf{R}_c)^{-1} \mathbf{R}_c^T \mathbf{Q}_c^{-1} \mathbf{R}_c \cdot \mathbf{A} \quad (28)$$

Suppose $\mathbf{R} = 0.5\times \mathbf{1}_{(N-1)\times(N-1)} + 0.5\mathbf{I}_{N-1}$ and let $\mathbf{Q}_{tcj} = \sigma_{tc}^2\mathbf{R}$, $\mathbf{Q}_{fcj} = \sigma_{fc}^2\mathbf{R}$, $\mathbf{Q}_t = \sigma_t^2\mathbf{R}$ and $\mathbf{Q}_f = \sigma_f^2\mathbf{R}$ represent the covariance matrices of the TDOA and FDOA measurements from the jth calibration source and the unknown emitter respectively, where σ_{tc}^2, σ_{fc}^2, σ_t^2 and σ_f^2 are the corresponding noise power. We get

$$\mathbf{R}_c^T \mathbf{Q}_c^{-1} \mathbf{R}_c = \begin{bmatrix} c^{-2} M \sigma_{tc}^{-2} \mathbf{R}^{-1} & \mathbf{0}_{(N-1)\times(N-1)} \\ \mathbf{0}_{(N-1)\times(N-1)} & \lambda^{-2} M \sigma_{fc}^{-2} \mathbf{R}^{-1} \end{bmatrix} \quad (29)$$

Substituting (29) in (28) yields

$$\mathbf{X}_{dc} = (1+\frac{\sigma_{tc}^2}{M\sigma_t^2})^{-1} CRLB(\boldsymbol{\theta})_t^{-1} + (1+\frac{\sigma_{fc}^2}{M\sigma_f^2})^{-1} CRLB(\boldsymbol{\theta})_f^{-1} \quad (30)$$

where $CRLB(\boldsymbol{\theta})_t = c^2(\mathbf{A}_t^T\mathbf{Q}_t^{-1}\mathbf{A}_t)^{-1}$, $\mathbf{A}_t = \partial\mathbf{r}/\partial\boldsymbol{\theta}$, $CRLB(\boldsymbol{\theta})_f = \lambda^2(\mathbf{A}_f^T\mathbf{Q}_f^{-1}\mathbf{A}_f)^{-1}$, $\mathbf{A}_f = \partial\dot{\mathbf{r}}/\partial\boldsymbol{\theta}$. $CRLB(\boldsymbol{\theta})_t$ and $CRLB(\boldsymbol{\theta})_f$ are the CRLB of $\boldsymbol{\theta}$ without receiver location errors using TDOA and FDOA respectively. Their values keep unvaried if the unknown emitter and the receivers are assigned.

Because $\mathbf{Y}_{dc}\mathbf{Z}_{dc}^{-1}\mathbf{Y}_{dc}^T$ is positive semi-definite, the optimal value of $\mathrm{cov}(\boldsymbol{\theta})$ is $\mathbf{X}_{dc}^{-1}$ when $\mathbf{Y}_{dc}\mathbf{Z}_{dc}^{-1}\mathbf{Y}_{dc}^T$ takes the value of zero. However, the optimal location accuracy is still worse than that without receiver location errors because $\sigma_{tc}^2 \neq 0$ and $\sigma_{fc}^2 \neq 0$ are always true. To restrain the performance degradation, adding the amount of the calibration sources is effective according to (30).

Equation (30) also shows that the optimal value of $\mathrm{cov}(\boldsymbol{\theta})$ increases along with the increase of σ_{tc}^2 and σ_{fc}^2.

As for $\mathbf{Y}_{dc}\mathbf{Z}_{dc}^{-1}\mathbf{Y}_{dc}^T > 0$, $\mathrm{cov}(\boldsymbol{\theta})$ is larger than $\mathbf{X}_{dc}^{-1}$ and the location accuracy becomes worse.

From the above analysis of differential calibration, we can conclude that improperly located calibration sources and large noise powers of TDOA and FDOA degrade the location accuracy. And the degradation could be so severe as to get a worse estimator of the unknown emitter than that without calibration sources.

IV. Simulations

In this section, we shall show through simulations how the location accuracy are influenced by the parameters of the calibration sources. The units used in the simulations are m for positions and m/s for velocities.

The position and the velocity of the unknown emitter are $\mathbf{u} = [600 \quad -650]^T$ and $\mathbf{v} = [-20 \quad 15]^T$. Six receivers are used to do the location task whose positions and velocities are listed below.

$\mathbf{s}_1 = [300 \quad 100]^T$, $\mathbf{v}_1 = [30 \quad -20]^T$

$\mathbf{s}_2 = [400 \quad 150]^T$, $\mathbf{v}_2 = [-30 \quad 10]^T$

$\mathbf{s}_3 = [300 \quad 500]^T$, $\mathbf{v}_3 = [10 \quad -20]^T$

$\mathbf{s}_4 = [350 \quad 200]^T$, $\mathbf{v}_4 = [10 \quad 20]^T$

$\mathbf{s}_5 = [-100 \quad -100]^T$, $\mathbf{v}_5 = [-20 \quad 10]^T$

$\mathbf{s}_6 = [200 \quad -300]^T$, $\mathbf{v}_6 = [20 \quad -10]^T$

A. Two-Dimensional Location Scenario with One Single Calibration Source

In the first simulation, we investigate the influence of the position to the location accuracy.

The TDOA and FDOA measurements from the unknown emitter and the calibration sources are obtained by adding Gaussian noise with $1ns$ to each true TDOA and $0.1Hz$ to each true FDOA respectively. The receiver location noises are set to be Gaussian noises with $\sigma_p = 1m$ and $\sigma_v = 0.7m/s$. Defining the performance gain as $G_{dc} = 1 - \sqrt{tr[\mathrm{cov}(\boldsymbol{\theta})]} \Big/ \sqrt{tr[CRLB(\boldsymbol{\theta})_s]}$, we get the trend of G_{dc} over calibration source position (x, y) in Fig. 2.

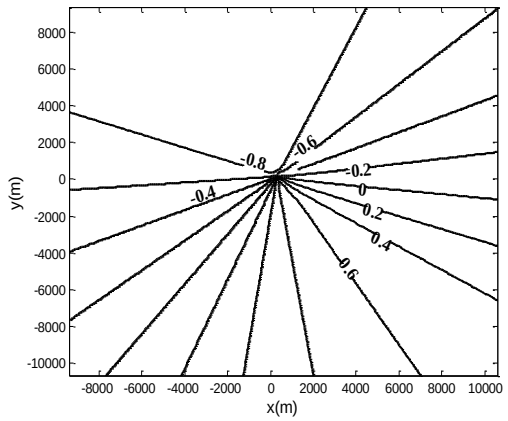

Fig. 2. Location accuracy gain.

Fig. 2 shows that there do exist some positions where the performance gain $G_{dc} < 0$. Because the differential calibration degrades the original accuracy at those positions, we must eliminate them .

The trend of G_{CRLB} over the calibration source position is in Fig. 3, where the performance gain G_{CRLB} is defined as $G_{CRLB} = 1 - \sqrt{tr[CRLB(\boldsymbol{\theta})]} \Big/ \sqrt{tr[CRLB(\boldsymbol{\theta})_s]}$.

Fig. 3 shows that the use of a single calibration source improves the location accuracy. Different position makes different gain and G_{CRLB} should not be lower than zero.

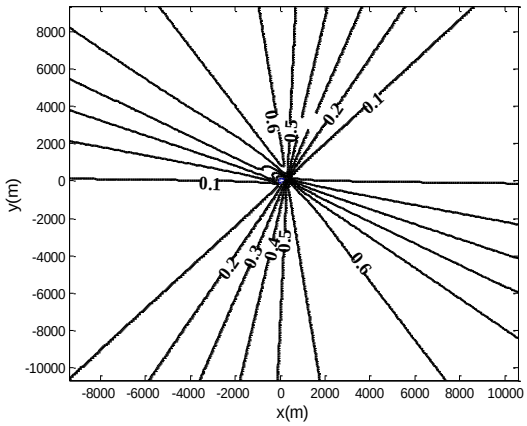

Fig. 3. Location accuracy gain.

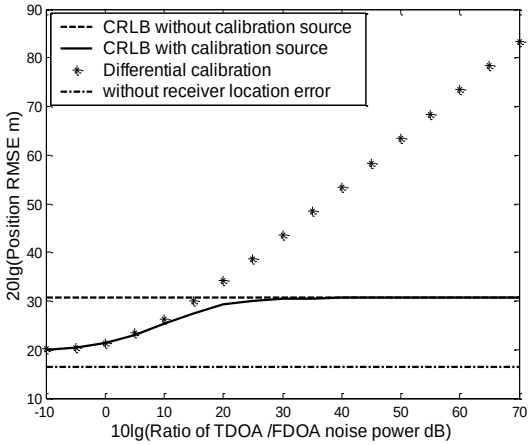

Fig. 4. Position accuracy curve.

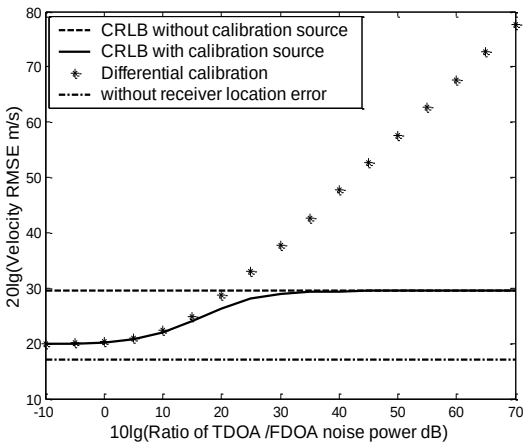

Fig. 5. Velocity accuracy curve.

In the second simulation, we investigate the influence of the accuracy of the TDOA and FDOA measurements from the calibration sources to the location accuracy.

The calibration source locates at $\mathbf{c}_1 = [600 \quad -326]^T$ where $G_{dc} = 0.6$. The statistics of the TDOA and FDOA measurements from the unknown emitter and those of the receiver location noises are the same as being defined in the first simulation. The trends of the location accuracy over the ratio of $10\lg(\sigma_{tc}^2/\sigma_t^2)$ where $\sigma_{fc}^2 = 0.1\sigma_{tc}^2$ are in Fig. 4 and Fig. 5.

Fig. 4 and Fig. 5 show that the location accuracy becomes worse as the noise powers of TDOA and FDOA measurements increase. Moreover, differential calibration provides performance gain when $10\lg(\sigma_{tc}^2/\sigma_t^2) < 20dB$. Yet, the CRLB curve with a calibration source shows properly used calibration source may not degrade the original location accuracy even if the measurements are too noisy to use.

B. Two-Dimensional Location Scenario with Multiple Calibration Sources

In the third simulation, we investigate the influence of the amount of the calibration sources to the location accuracy.

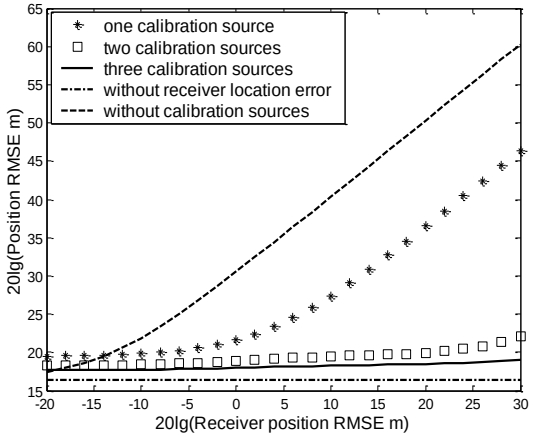

Fig. 6. Position accuracy curve.

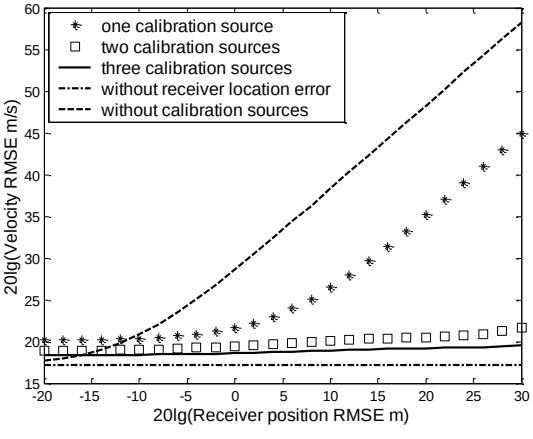

Fig. 7. Velocity accuracy curve.

The statistics of the TDOA and FDOA measurements from the unknown emitter and the calibration sources are the same as those in the first simulation. Fig. 6 and Fig. 7 show the trends of the location accuracy over the receiver location errors. The velocity noise power σ_v^2 is set to be half of the position noise power σ_p^2 which varies as $-20dB \le 10\lg\sigma_p^2 \le 30dB$.

By use of the calibration source $\mathbf{c}_1$ selected in the second simulation according to Fig. 2, differential calibration provides performance gain at large receiver location errors. Though the gain increases along with the increase of the calibration source number, the increment between j sources and j+1 sources becomes less as j becomes larger.

Differential calibration fails to provide performance gain when the receiver location errors are small. The threshold depresses as the calibration source number increases. For example, it is −12dB for one calibration source and −16dB for two sources as is shown in Fig. 6.

The other two calibration sources used in the third simulation are located at $\mathbf{c}_2 = [500 \quad -427]^T$ and $\mathbf{c}_3 = [1000 \quad -1528]^T$. The position optimization process is illustrated in Appendix B.

In the fourth simulation, we compare the location accuracy of these three calibration sources with that of arbitrary distributed ones located at $\mathbf{c}_4 = [600 \quad 184]^T$, $\mathbf{c}_5 = [400 \quad 120]^T$ and $\mathbf{c}_6 = [1000 \quad 200]^T$.

The statistics of the TDOA and FDOA measurements from the unknown emitter and the calibration sources are the same as those in the first simulation.

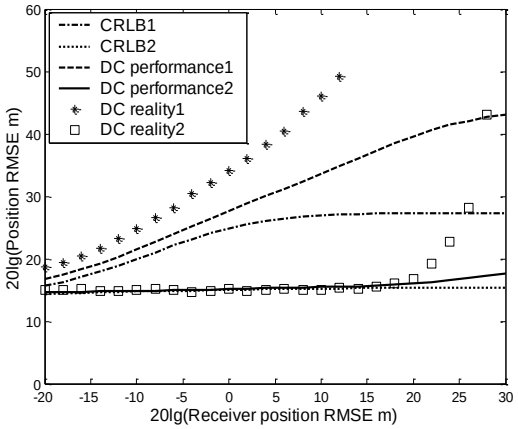

Fig. 8. Position accuracy curve.

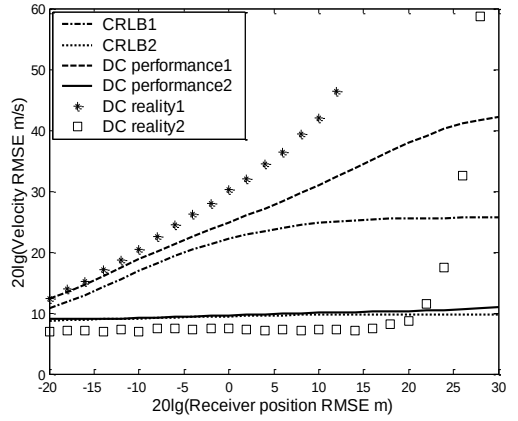

Fig. 9. Velocity accuracy curve.

Fig. 8 and Fig. 9 show the trends of the location accuracy over the receiver location errors defined in the third simulation. The curves marked as "1" represents the calibration source group $\mathbf{p}_1 = [\mathbf{c}_4^T \quad \mathbf{c}_5^T \quad \mathbf{c}_6^T]^T$ and those marked as "2" represents $\mathbf{p}_2 = [\mathbf{c}_1^T \quad \mathbf{c}_2^T \quad \mathbf{c}_3^T]$.

$tr[\mathrm{cov}(\boldsymbol{\theta})] > tr[CRLB(\boldsymbol{\theta})]$ is permanent established in the same location scenario. Using optimized calibration sources provides better location accuracy which is close to the CRLB. And the convergence can be ensured for large receiver position and velocity errors after the calibration source position optimization.

V. Conclusions

This paper investigated through CRLB analysis the performance of differential calibration algorithm in the presence of receiver location uncertainty. It gives out the performance equation of differential calibration algorithm and reveals that differential calibration may not provide performance gain if the amount and positions of the calibration sources are badly selected. When the amount and positions are selected properly, the measurements from the calibration sources must be accurate enough to improve the location accuracy.

Appendix A Important Variables

The values of matrices $\mathbf{A}$, $\mathbf{D}$ and $\mathbf{D}_c$ is essential to get the simulation results. They are listed as follows.

Suppose $\mathbf{A} = [\mathbf{A}_t^T \quad \mathbf{A}_f^T]^T$. The kth row of $\mathbf{A}_t$ and $\mathbf{A}_f$ are $\mathbf{A}_{tk}$ and $\mathbf{A}_{fk}$ respectively. Their values are

$$\mathbf{A}_{tk} = (\partial r_{uk}/\partial \boldsymbol{\theta})^T = [(\mathbf{b}_{k+1}^T - \mathbf{b}_1^T) \quad \mathbf{0}_{1\times 3}]$$
$$\mathbf{A}_{fk} = (\partial \dot{r}_{uk}/\partial \boldsymbol{\theta})^T = [(\mathbf{q}_{k+1}^T - \mathbf{q}_1^T) \quad (\mathbf{b}_{k+1}^T - \mathbf{b}_1^T)].$$

where $\mathbf{q}_i = (\mathbf{v} - \mathbf{v}_i)/r_i - (\mathbf{v} - \mathbf{v}_i)^T \mathbf{b}_i \cdot (\mathbf{u} - \mathbf{s}_i)/r_i^2$.

The kth and $(k+N-1)th$ rows of $\mathbf{D}$ are

$$(\partial r_{uk}/\partial \boldsymbol{\beta})^T = [\mathbf{b}_1^T \quad \mathbf{0}_{1\times 3(k-1)} \quad -\mathbf{b}_{k+1}^T \quad \mathbf{0}_{1\times 3(N-k-1)} \quad \mathbf{0}_{1\times 3N}]$$
$$(\partial \dot{r}_{uk}/\partial \boldsymbol{\beta})^T = [\mathbf{D}_{fqk} \quad \mathbf{D}_{fbk}].$$

where $\mathbf{D}_{fqk} = [\mathbf{q}_1^T \quad \mathbf{0}_{1\times 3(k-1)} \quad -\mathbf{q}_{k+1}^T \quad \mathbf{0}_{1\times 3(N-k-1)}]$ and $\mathbf{D}_{fbk} = [\mathbf{b}_1^T \quad \mathbf{0}_{1\times 3(k-1)} \quad -\mathbf{b}_{k+1}^T \quad \mathbf{0}_{1\times 3(N-k-1)}]$.

The $[j(N-1)+k]th$ and $[(j+M)(N-1)+k]th$ rows of $\mathbf{D}_c$ are

$$(\partial r_{cjk}/\partial \boldsymbol{\beta})^T = \left[\mathbf{b}_{cj1}^T \quad \mathbf{0}_{1\times 3(k-1)} \quad -\mathbf{b}_{cj(k+1)}^T \quad \mathbf{0}_{1\times 3(N-k-1)} \quad \mathbf{0}_{1\times 3N}\right],$$
$$(\partial \dot{r}_{cjk}/\partial \boldsymbol{\beta})^T = [\mathbf{D}_{cfqk} \quad \mathbf{D}_{cfbk}].$$

where

$$\mathbf{D}_{cfqk} = [\mathbf{q}_{cj1}^T \quad \mathbf{0}_{1\times 3(k-1)} \quad -\mathbf{q}_{cj(k+1)}^T \quad \mathbf{0}_{1\times 3(N-k-1)}]$$
$$\mathbf{q}_{cji} = -\mathbf{v}_i/r_{ji} + \mathbf{v}_i^T \mathbf{b}_{cji} \cdot (\mathbf{c}_j - \mathbf{s}_i)/r_{ji}^2$$
$$\mathbf{D}_{cfbk} = [\mathbf{b}_{cj1}^T \quad \mathbf{0}_{1\times 3(k-1)} \quad -\mathbf{b}_{cj(k+1)}^T \quad \mathbf{0}_{1\times 3(N-k-1)}].$$

Appendix B Position Optimization

According to the value of G_{dc}, select an optimal point in Fig. 2 as the first calibration source position. Ensure

the possible positions of the second calibration source and repeat the computation of G_{dc} with two calibration sources. Fig. 10 shows the trends of the location accuracy over the second calibration source position.

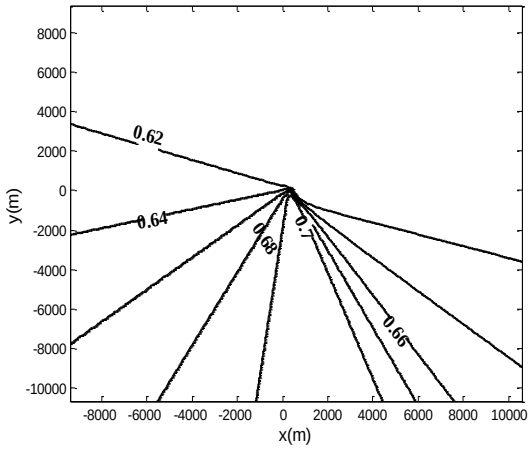

Fig. 10. Location accuracy gain.

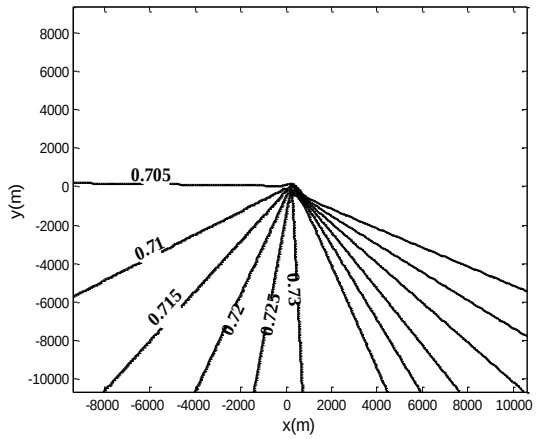

Fig. 11. Location accuracy gain.

From Fig. 10, we can see that the first choice of $\mathbf{c}_1$ is important because the optimal position makes it easy to select the second one. Repeat the above operation and compute G_{dc} with three calibration sources. Fig. 11 shows the trends of the location accuracy over the third calibration source position.

Fig. 11 shows that the location accuracy increases with less increment than the former. Select a possible position in Fig. 11 and we get three calibration sources used in the third simulation.

REFERENCES

[1] K. C. Ho and Wenwei Xu, "An accurate algebraic solution for moving source location using TDOA and FDOA measurements," *IEEE Trans. on Signal Processing*, vol. 52, pp. 2453-2463, September 2004.

[2] H. G. Yu, G. M. Huang, J. Gao, and B. Liu, "An efficient constrained weighted least squares algorithm for moving source location using TDOA and FDOA measurements," *IEEE Trans. on Wireless Communications*, vol. 11, pp. 44-47, January 2012.

[3] C. Li, C. F. Liu, G. S. Liao, and Y. B. Li, "Solution and analysis of constrained least square passive location algorithm," *Systems Engineering and Electronics*, vol. 34, pp. 221-226, February 2012.

[4] X. J. Jia, F. C. Guo, and Y. Y. Zhou, "Performance analysis of triple-observer passive localization using FDOA measurements," *Signal Processing*, vol. 27, pp. 600-605, April 2011.

[5] K. C. Ho, X. N. Lu, and L. Kovavisaruch, "Source localization using TDOA and FDOA measurements in the presence of receiver Location errors: analysis and solution," *IEEE Trans. on Signal Processing*, vol. 55, pp. 684-696, February 2007.

[6] W. Z. Qu, S. F. Ye, and Z. B. Sun, "Algorithm of position calibrator for satellite interference location," *Chinese Journal of Radio Science*, vol. 20, pp. 342-346, June 2005.

[7] H. Yan and S. F. Yao, "Calibration accuracy analysis of LEO dual-satellite geolocation system based on reference stations," *Telecommunication Engineering*, vol. 51, pp. 27-33, December 2011.

[8] K. C. Ho and L. Yang, "On the use of a calibration emitter for source localization in the presence of sensor position uncertainty," *IEEE Trans. on Signal Processing*, vol. 56, pp. 5758-5772, December 2008.

[9] S. M. Kay, P. F. Luo, *et al.*, *Foundamentals of Statistical Signal Processing*, Beijing, CHN: Publish House of Electronics Industry, 2011, pp. 110-117.

[10] X. D. Zhang, *Matrix Analysis and Applications*, Beijing, CHN: Tsinghua University Press, 2004, pp. 64-71.

[11] J. B. Jin, N. Wu, and Q. Yang, "Sensor placement strategies for TDOA location system based on semidefinite relaxation," *Journal of Circuits and Systems*, vol. 18, pp. 134-138, April 2013.

Li Zhang was born in Jiangxi Province, China, in 1975. She received the B.E. and M.E. degrees in communication engineering from the Institute of Zhengzhou Information Science and Technology, Zhengzhou, China, in 1997 and 2000, respectively. She is currently working towards the Ph.D. degree at the same institute. Her research interests include passive location, signal detection and digital signal processing.

Ding Wang was born in Anhui Province, China. He received the B.E., M.E. and D.E. degrees in communication engineering from the Institute of Zhengzhou Information Science and Technology, Zhengzhou, China, in 2004, 2007 and 2012, respectively. His research interests include array signal processing and passive location.

Ying Wu was born in Henan Province, China. She received the B.E. degree in communication engineering from the Institute of Zhengzhou Information Science and Technology, Zhengzhou, China, in 1982. She then received the M.E. degree in communication engineering from Beijing Institute of Technology, Beijing, China, in 1985. Her research interests include array signal processing, passive location, signal detection and digital signal processing.

